Physica B 404 (2009) 706–709

Contents lists available at ScienceDirect

Physica B

journal homepage: www.elsevier.com/locate/physb

Effect of the double doping mechanism on the phase diagram of $Y_{1-x}Ca_xBa_2Cu_3O_{6+y}$

Francesco Coneri [a], Giorgio Concas [b], Sean Giblin [c], Americo Rigoldi [b], Samuele Sanna [a], Roberto De Renzi [a,*]

[a] Dipartimento di Fisica and CNISM, Università di Parma, Viale Usberti, 7A, I-43100 Parma, Italy
[b] Dipartimento di Fisica and CNISM, Università di Cagliari, Monserrato-Sestu, Km 0.7, I-09042 Monserrato (CA), Italy
[c] ISIS Facility, Rutherford Appleton Lab., Chilton, Didcot OX11 0QX, UK

ARTICLE INFO

Keywords:
Cuprate superconductors
Metal insulator transition
Disorder

ABSTRACT

We investigated the effect of hole doping and quenched disorder on the phase diagram of $Y_{1-x}Ca_xBa_2Cu_3O_{6+y}$, by exploiting the double doping mechanism of Y–Ca substitution and O intercalation in the undoped-to-heavily underdoped regime. We show that the insulator to metal transition, governed by the mobile hole concentration, reflects only the charges transferred by chain oxygen (the y fraction in the chemical formula). The transition is preceded by the suppression of antiferromagnetic order, which is replaced by a cluster spin glass ground state. We discuss the effect of doping and disorder on both magnetic states and on the appearance of superconductivity.

1. Introduction

The main physical parameter determining the characteristic phase diagram of cuprates high T_c superconductors is the density h of mobile holes in the active CuO_2 layers. The phase diagrams present *universal* features, common to all families of cuprates, starting from a parent insulating antiferromagnet (AF) compound of given Néel temperature T_N^o at $h=0$, including the suppression of AF order at some critical value h_{c1}, the appearance of superconductivity (SC) at h_{c2}, and a dome-shaped $T_c(h)$ with an optimal T_c^o at h_o. However, closer inspection reveals that different families present subtle differences, most notably in the values of T_c^o and T_N^o [1], but also in position of the critical densities $h_{c1,c2}$. In particular h_{c1} and h_{c2} may nearly coincide, as in $YBa_2Cu_3O_{6+y}$ [2], or most often differ significantly, opening a window of cluster spin glass (CSG) in the phase diagram. The CSG phase is characterized by magnetic order with static short range AF correlations below a transition temperature $T_g \ll T_N^o$.

The mechanisms at the origin of these differences are investigated in the hope that their understanding may help clarifying the persisting mysteries of high T_c superconductivity. One of the candidates mechanism is quenched disorder. It is intrinsic in the doping of many cuprates, where the substitution of trivalent with divalent cations injects holes into the active layers, but it also introduces a random local variation in the lattice.

$YBa_2Cu_3O_{6+y}$ is the material of choice as a starting point for this investigation, being the closest to the clean limit [2–4]. This compound shares the crystal structure with $Y_{1-x}Ca_xBa_2Cu_3O_{6+y}$, where disorder is introduced in a nearest neighbor block to the active layers by the charged heterovalent (M = Ca) substitution, which is also expected to provide an additional contribution to the mobile holes. We investigated different families of this second compound, at fixed Ca (hence fixed disorder) and variable O content, from the undoped to the heavily underdoped SC regime. A related topic was already addressed in an earlier seminal work [5] on $Y_{1-x}Ca_xBa_2Cu_3O_6$, where, however, doping and disorder are linked by a single control parameter (x).

Here the hole density h, experimentally determined from thermopower measurements [6] at room temperature (RT), has two independently tunable sources, calcium and oxygen ($h = h^{Ca}(x) + h^{O}(y)$), each of which[1] is a distinct function of its respective stoichiometry, x and y.

The aim of our investigation is to vary both doping and disorder in controlled fashion, in order to pinpoint specific differences in the magnetic and/or in the superconducting sectors of the phase diagram.

2. Experimental

Polycrystalline samples were produced by a standard topotactic technique [7]. The dominant compositional uncertainty stems from that of the oxygen content ($\delta y = \pm 0.01$) of the two precursors in the topotactic sealed-vessel equilibration, a fully oxidized and a fully reduced sample in stoichiometric proportions,

* Corresponding author. Tel.: +39 521 905 279; fax: +39 521 905 223.
E-mail address: roberto.derenzi@unipr.it (R. De Renzi).

[1] Superscripts distinguish these partial densities, subscripts identify their critical an optimal values.

0921-4526/$ - see front matter © 2008 Elsevier B.V. All rights reserved.
doi:10.1016/j.physb.2008.11.193

appearing therefore as a small random error between families. Composition was checked by X-ray and neutron diffraction; thermopower was calibrated to yield the RT (295 K) total mobile hole density h. SQUID magnetometry in a field of 0.2 mT provided T_c, as the linear extrapolation of the drop of susceptibility, from 10% to 90% of the lowest temperature value. μSR experiments were performed at ISIS on the EMU and MUSR beamlines, in transverse field (TF) to yield superconducting properties (see Ref. [8] for a more extensive report) and in zero field (ZF) to detect magnetic order below T_N or T_g.

Fig. 1 shows the typical appearance of the ZF muon time dependent asymmetry $A(t)$ in non-superconducting samples, with $T_N = 280$ K in (a) and with $T_g = 20$ K in (b). A small cryostat contribution has been subtracted and the best fit functions are:

$$A(t) = A_0 e^{-t/T_1} e^{-\sigma_n^2 t^2/2} \quad (1)$$

for $T > T_{N,g}$, where A_0 is the full experimental asymmetry from the sample, and

$$A(t) = \sum_{i=1}^{n} (A_{Li} e^{-t/T_i} + A_{Ti} e^{-\sigma_i^2 t^2/2} \cos \omega_{\mu i} t) \quad (2)$$

for $T \ll T_{N,g}$. In Eq. (1) the full asymmetry is non-precessing (it measures the *longitudinal* projection of the muon spin along its initial direction) and the relaxation accounts for both paramagnetic fluctuations (with rate $1/T_1$) and static nuclear spins (with Gaussian rate σ_n)); in Eq. (2) the sum is over the two

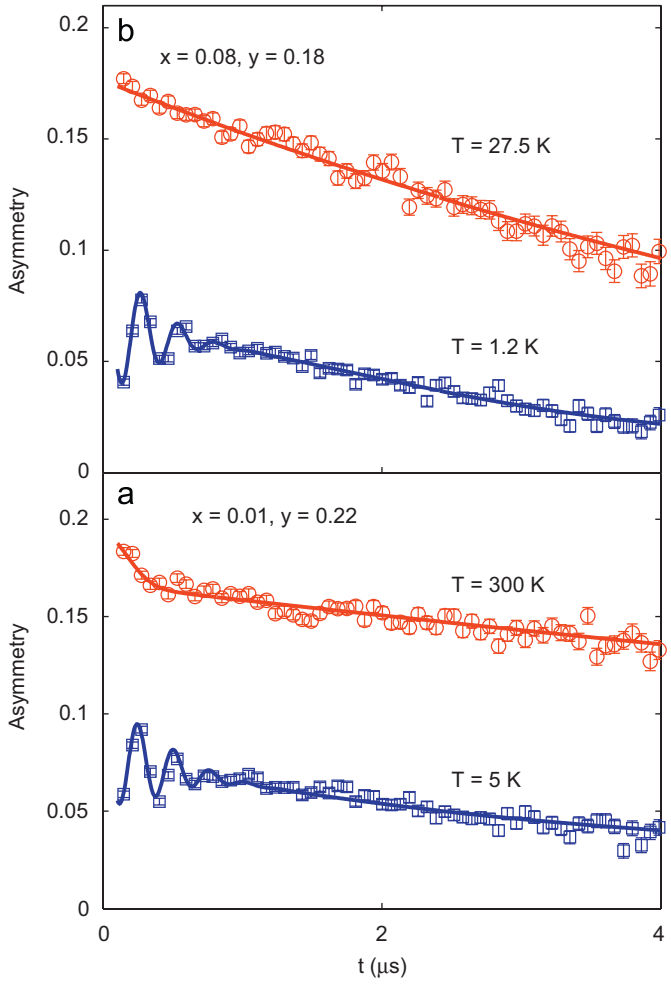

Fig. 1. Muon asymmetries above (○) and well below $T_{N,g}$ (□) for (a) $x = 0.01$ and $y = 0.22$, ($T_N = 280$ K); (b) $x = 0.08$ and $y = 0.18$ ($T_g = 20$ K); the curves are the best fits to Eqs. (1) and (2).

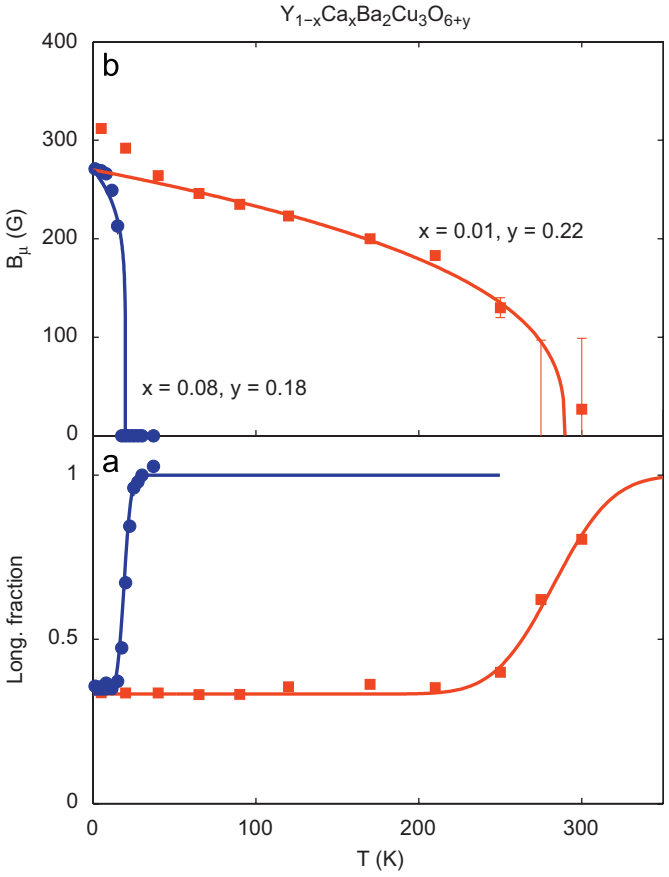

Fig. 2. (a) Drop of the longitudinal asymmetry vs. temperature for two typical AF ($x = 0.01, y = 0.22$) and CSG ($x = 0.08, y = 0.18$) samples (curves are best fits, see text). (b) Corresponding internal field.

different muon stopping sites [9–11], giving rise to both longitudinal terms, with asymmetries A_{Li}, and *transverse* terms, with asymmetries A_{Ti}, due to precessions at frequencies $\omega_{\mu i} = 2\pi\gamma_\mu B_{\mu i}$, around internal fields $B_{\mu i}$, with $\gamma_\mu = 135.5$ MHz/T. Geometrical average over random powder orientations leads to the total longitudinal asymmetry obeying $\sum_i A_{Li} = A_0/3$ for $T < T_{N,g}$, whereas the transverse asymmetry, which should add to $2A_0/3$, is partially missing.

The magnetic transition is marked by a sharp drop of the total longitudinal asymmetry around $T_{N,g}$, from A_0 to $A_0/3$. Fig. 2(a) shows the drop of the non-precessing component, which would be a step at $T_{N,g}$ in the ideal case, whereas it is fitted to an error function, representing a Gaussian distribution of Néel temperatures in the polycrystal samples. As it is shown in Fig. 2(b) the internal field corresponding to the larger asymmetry, $B_{\mu 1}$, vanishes around the mean of this distribution, which we take as the experimental transition temperature. Both the AF and CSG phase allow similar procedures, i.e. the static internal fields do not distinguish the two states (see Fig. 1), the spin glass being characterized only by the low ordering temperature. The boundary between the two states corresponds to a sharp jump in the derivative of the transition temperature with respect to doping, quite apparent from the phase diagram discussed below.

3. Discussions

The main panel in Fig. 3 displays the dependence of the transition temperatures T_N, T_g and T_c on the oxygen content y, which is proportional to the *varying* h^O density of charges